

Charge Exchange Spin-Dipole Excitations of ^{90}Zr and ^{208}Pb and Neutron Matter Equation of State

H. Sagawa ^a, Satoshi Yoshida ^b, Xian-Rong Zhou^c, K. Yako ^d, and H. Sakai ^d

^a *Center for Mathematical Sciences,
the University of Aizu, Aizu-Wakamatsu,
Fukushima 965-8580, Japan*

^b *Science Research Center,
Hosei University 2-17-1 Fujimi,
Chiyoda, Tokyo 102-8160, Japan*

^c *Department of Physics and Institute
of Theoretical Physics and Astrophysics,
Xiamen University,
Xiamen 361005, P. R. China*

^d *Department of Physics,
University of Tokyo, Bunkyo,
Tokyo 113-0033, Japan*

(Dated: January 11, 2019)

Abstract

Charge exchange spin-dipole (SD) excitations of ^{90}Zr and ^{208}Pb are studied by using a Skyrme Hartree-Fock(HF) + Random Phase approximation (RPA). The calculated spin-dipole strength distributions are compared with experimental data obtained by ^{90}Zr (p,n) ^{90}Nb and ^{90}Zr (n,p) ^{90}Nb reactions. The model-independent SD sum rule values of various Skyrme interactions are studied in comparison with the experimental values in order to determine the neutron skin thickness of ^{90}Zr . The pressure of the neutron matter equation of state (EOS) and the nuclear matter symmetry energy are discussed in terms of the neutron skin thickness and peak energies of SD strength distributions.

PACS numbers: 24.30.Cz, 21.10.Pc, 23.20.Lv, 21.60.Jz

I. INTRODUCTION

The relationship between the neutron matter equation of state (EOS) and the neutron skin thickness has been studied extensively by using the Skyrme Hartree-Fock (HF) model, a relativistic mean field (RMF) model [1, 2, 3]. The neutron matter EOS is essential for studying the properties of neutron stars, e.g., their size [4]. It is also known that isovector nuclear matter properties, including the symmetry energy, correlate strongly with the neutron skin thickness in heavy nuclei [2, 5, 6].

Elastic electron scattering has provided accurate data on the charge distributions of nuclei. Several experimental attempts have been made to measure neutron distributions, for example, by proton elastic scattering [7, 8, 9, 10] and by inelastic alpha scattering to giant dipole resonance excitations [11]. However, empirical results of neutron skin thickness obtained by proton scattering are controversial and do not agree with each other even within experimental error. The accuracy of empirical data on neutron distributions from giant resonance experiments is also rather poor, insufficient to extract accurate information on the neutron matter EOS. One promising tool for studying neutron distributions is the parity violation electron scattering experiment [12]. Unfortunately, no data on parity violation electron scattering experiments is available so far.

The model-independent sum rule strength of charge exchange SD excitation is directly related to information on the neutron skin thickness [13]. Recently, SD excitations were studied in ^{90}Zr by the charge exchange reactions $^{90}\text{Zr}(p,n)^{90}\text{Nb}$ [14] and $^{90}\text{Zr}(n,p)^{90}\text{Y}$ [15], and the model-independent sum rule strengths for the SD excitations were extracted in Ref. [16] by using multipole decomposition (MD) analysis [17]. The charge exchange reactions $(^3\text{He},t)$ on Sn isotopes were also studied to extract the neutron skin thickness [18]. However, one needs the counter experiment $(t,^3\text{He})$ or (n,p) on Sn isotopes in order to extract the model-independent sum rule value from experimental data. This counter experiment is missing in the case of Sn isotopes.

It is known that the SD strength has almost the same amount of contributions to neutrino reactions as that of the Gamow-Teller strength [19]. The Pb target is considered to be the most promising candidate for detecting the heavy-flavor neutrinos from the supernovae. Thus, it is quite important to study the SD strength in the Pb target for a precise evaluation of the cross-sections of charge-induced neutrino reactions.

In this paper, we study the SD excitations and the neutron skin thickness by using the HF and HF+ random phase approximation (RPA) with Skyrme interactions. As a theoretical model, the HF+RPA model has been extensively applied to giant resonances in a broad region of mass table[20, 21]. The same model was used for the study of spin-dependent charge exchange excitations[22, 24, 25, 26]. It was shown that the model successfully predicts GT and SD states in ^{48}Sc and ^{90}Nb [24, 25]. First, we calculate the SD states in nuclei with mass $A=90$ and 208 by using the charge exchange HF + RPA model with various Skyrme interactions. We will compare calculated results of SD strength distributions with empirical data obtained by charge exchange (p,n) and (n,p) reactions on ^{90}Zr . The sum rule values are also compared with the empirical values in Section 2. Next, the correlations between the neutron matter EOS and the SD sum rules are studied in the Skyrme HF model. We will discuss the neutron matter EOS by using the experimental SD data and other empirical information on the neutron skin. This paper is organized as follows. In Section 2, the SD strength of the HF+RPA calculations is presented for both the t_- and t_+ isospin channels on ^{90}Zr and ^{208}Pb . The calculated results are compared with experimental results of $^{90}\text{Zr}(\text{p,n})^{90}\text{Nb}$ and $^{90}\text{Zr}(\text{n,p})^{90}\text{Y}$ reactions. We study the correlations between the sum rules of SD strength and the pressure of neutron matter EOS in Section 3. A summary is given in section 4.

II. HF+RPA CALCULATIONS OF SD STRENGTH

The operators for SD transitions are defined as

$$\hat{S}_{\pm} = \sum_{im\mu} t_{\pm}^i \sigma_m^i r_i Y_1^{\mu}(\hat{r}_i) \quad (1)$$

with the isospin operators $t_3 = t_z$, $t_{\pm} = (t_x \pm it_y)$. The model-independent sum rule for the λ -pole SD operator $\hat{S}_{\pm}^{\lambda} = \sum_i t_{\pm}^i r_i [\sigma \times Y_1(\hat{r}_i)]^{\lambda}$ can be obtained as

$$\begin{aligned} S_{-}^{\lambda} - S_{+}^{\lambda} &= \sum_{i \in \text{all}} |\langle i | \hat{S}_{-}^{\lambda} | 0 \rangle|^2 - \sum_{i \in \text{all}} |\langle i | \hat{S}_{+}^{\lambda} | 0 \rangle|^2 \\ &= \langle 0 | [\hat{S}_{-}^{\lambda}, \hat{S}_{+}^{\lambda}] | 0 \rangle = \frac{(2\lambda + 1)}{4\pi} (N \langle r^2 \rangle_n - Z \langle r^2 \rangle_p). \end{aligned} \quad (2)$$

The sum rule for the spin-dipole operator (1) then becomes

$$S_{-} - S_{+} = \sum_{\lambda} (S_{-}^{\lambda} - S_{+}^{\lambda}) = \frac{9}{4\pi} (N \langle r^2 \rangle_n - Z \langle r^2 \rangle_p). \quad (3)$$

It should be noted that the sum rule (3) is directly related to the difference between the mean square radius of neutrons and protons with the weight of neutron and proton numbers. We adopt four Skyrme interactions, namely, SIII, SGII, SkI3 and SLy4, for the HF+RPA calculations. The Landau parameters and nuclear matter properties of these interactions are shown in Table I. For the spin-isospin excitations, the value G'_0 plays the important role of determining the collective properties of the excitation [22]. The RPA equation is solved using the basis expanded by the harmonic oscillator wave functions up to the maximum major quantum number of $N_{max}=10$ for ^{90}Zr and $N_{max}=12$ for ^{208}Pb . The HF calculations are performed without the spin-gradient terms (J^2 terms) since the adopted Skyrme interactions have been fitted without them [22, 23], but the RPA calculations incorporate the spin-gradient terms. The two-body spin-orbit and two-body Coulomb interactions are neglected in the RPA calculations. We also performed the continuum HF+RPA calculations with one of the interactions and found essentially the same strength distributions as in the present calculations except the width due to the coupling to the continuum [21]. The calculated results are smoothed out by using a weighting function, ρ :

$$\frac{dB(SD)_{ave}}{dE_x} = \int \frac{dB(SD)}{dE'_x} \rho(E'_x - E_x) dE'_x \quad (4)$$

where the weighting function is defined as

$$\rho(E'_x - E_x) = \frac{1}{\pi} \frac{\Delta/2}{(E'_x - E_x)^2 + (\Delta/2)^2} \quad (5)$$

taking the width parameter Δ . In the present calculations with the discrete basis, the SD strength is given by

$$\frac{dB(SD)}{dE'_x} = \sum_i B(SD; E_i) \delta(E_i - E'_x).$$

A. Charge exchange SD excitations of ^{90}Zr

The HF calculations are performed by using four Skyrme interactions in Table I. The proton, charge and neutron radii of ^{90}Zr are listed in Table II together with the sum rule values $\Delta S = S_- - S_+$ calculated through the analytic equation (3). By using the same HF wave functions, the charge exchange RPA calculations give the SD strengths in ^{90}Nb and ^{90}Y excited by the $t_{\pm} r \sigma Y_1(\hat{r})$ operators from the parent nucleus ^{90}Zr , as shown in Figs. 1 and 2. The experimentally obtained distributions of the SD strengths are also plotted in Figs.

TABLE I: Landau parameters, effective mass m^* and symmetry energy J of Skyrme interactions

	SIH	SGII	SkI3	SLy4
F_0	0.309	-0.235	-0.318	-0.273
F'_0	0.862	0.733	0.653	0.818
G_0	0.052	0.014	0.569	1.120
G'_0	0.457	0.509	0.203	-0.138
F_1	-0.709	-0.646	-1.269	-0.926
F'_1	0.490	0.521	-0.843	-0.399
G_1	0.490	0.612	1.33	0.279
G'_1	0.490	0.432	0.65	1.047
m^*/m	0.76	0.78	0.58	0.69
$J(\text{MeV})$	28.1	26.9	34.8	32.3

1 and 2. The experimental SD strength distributions for the t_- and the t_+ channels were obtained from the $^{90}\text{Zr}(p,n)^{90}\text{Nb}$ and the $^{90}\text{Zr}(n,p)^{90}\text{Y}$ data, respectively, by performing MD analysis [16]. A comprehensive description of the MD analysis can be found in ref. [17].

TABLE II: Proton, neutron and charge radii of ^{90}Zr . The charge radius is obtained by folding the proton finite size. The sum rule values $\Delta S = S_- - S_+$ of spin-dipole excitations are calculated by Eq. (3) with the HF neutron and proton mean square radii. Experimental data on the charge radius are taken from ref. [27]. The experimental values $r_n - r_p$ are taken from [7, 16]. The radii are given in units of fm, while the SD sum rules are given in units of fm^2 .

	SIH	SGII	SkI3	SLy4	exp
r_p	4.257	4.198	4.174	4.225	—
r_c	4.321	4.263	4.240	4.290	4.258 ± 0.008
r_n	4.312	4.253	4.280	4.287	—
$r_n - r_p$	0.055	0.055	0.106	0.064	0.09 ± 0.07 [7], 0.07 ± 0.04 [16]
ΔS	146.7	142.9	156.9	146.9	

In general, the t_- SD strength distributions for 0^- and 1^- states in ^{90}Nb are concentrated in one state at $E_x \sim 30\text{MeV}$, having a large portion of the non-energy weighted sum rule (NEWSR) strength, while those for the 2^- states are separated into two dominant peaks, as

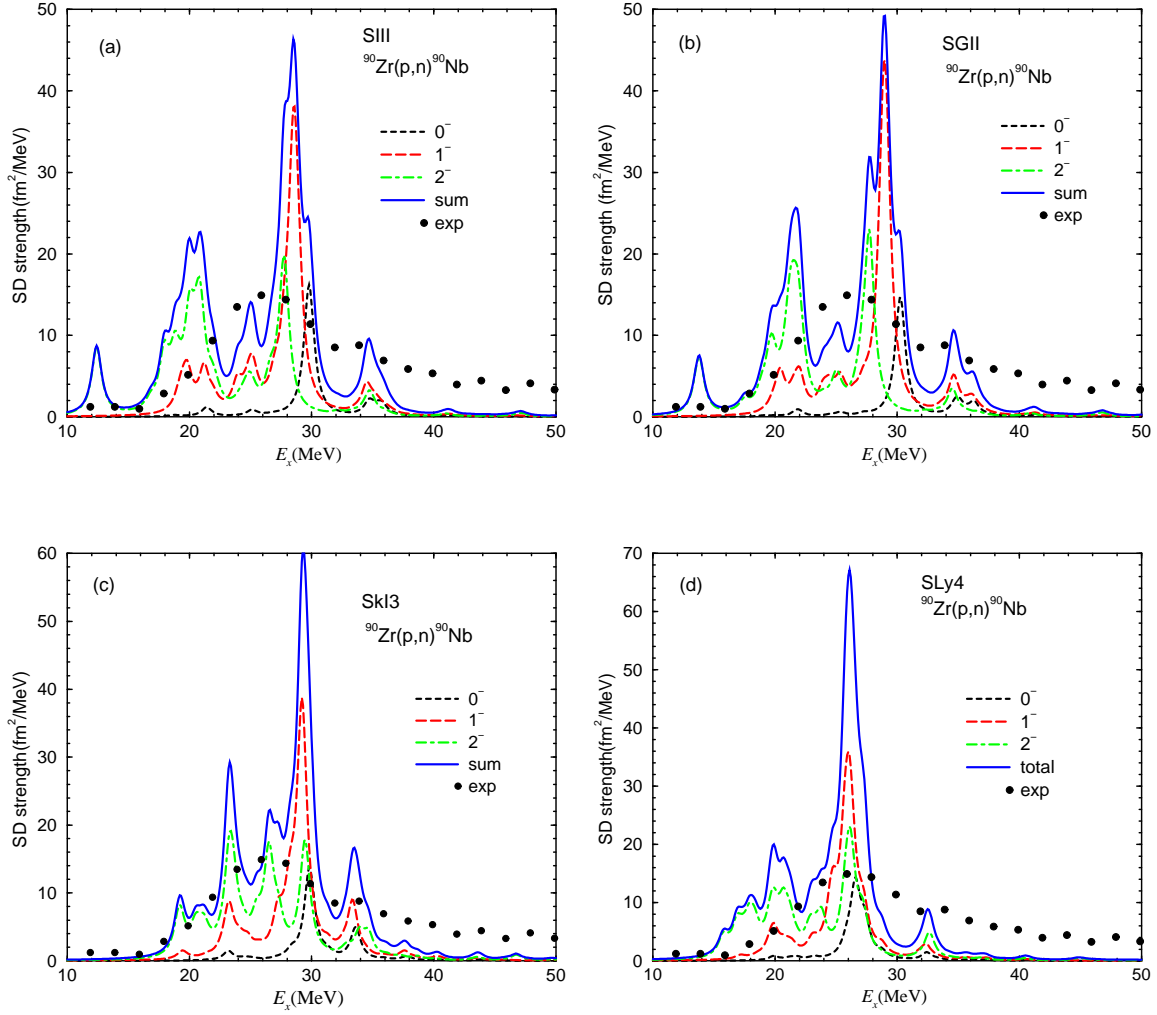


FIG. 1: (Color online) Charge exchange SD strengths for the operators $\hat{S}_{-}^{\lambda} = \sum_i t_{-}^i r_i [\sigma \times Y_1(\hat{r}_i)]^{\lambda}$ calculated by the HF+RPA model with the Skyrme interactions (a) SIII, (b) SGII, (c) SkI3 and (d) SLy4. The excitation energy is referred to the ground state of the parent nucleus ^{90}Zr . The dotted, dashed and long-dashed lines show the SD strengths of $\lambda = 0^{-}, 1^{-}$ and 2^{-} , respectively, while the solid curve shows the sum of three multipoles. The SD strength is averaged by the weighting function (5) with the width $\Delta=1\text{MeV}$. The experimental data shown by the black dots are taken from ref. [16].

shown in Fig. 1. The 0^{-} peak appears at $E_x \sim 30\text{MeV}$, having 73%, 65%, and 58% of the NEWSR value for the SIII, SGII and SkI3 interactions, respectively. The calculated results for 1^{-} states show a peak at $E_x \sim 29\text{MeV}$ having 50%, 59% and 48% of the NEWSR value

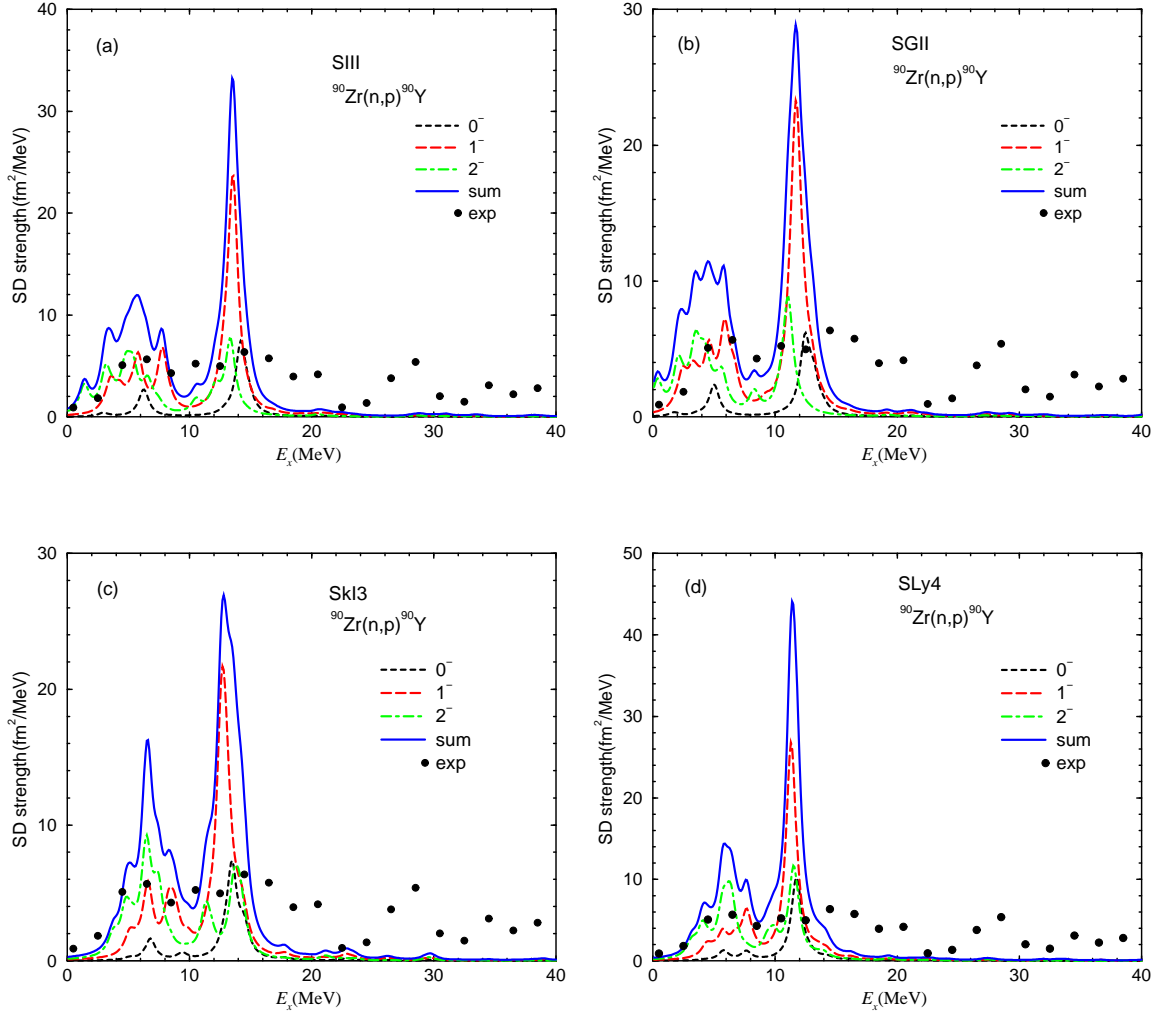


FIG. 2: (Color online) Charge exchange SD strengths for the operators $\hat{S}_+^\lambda = \sum_i t_+^i r_i [\sigma \times Y_1(\hat{r}_i)]^\lambda$ calculated by the HF+RPA model using the Skyrme interactions (a) SIII, (b) SGII, (c) SkI3 and (d) SLy4. The excitation energy is referred to the ground state of the parent nucleus ^{90}Zr . The SD strength is averaged by the weighting function (5) with a width of $\Delta=1\text{MeV}$. The experimental data shown by the black dots are taken from ref. [16]. See the captions to Fig. 1 for details.

for the SIII, SGII and SkI3 interactions, respectively. The three results in Figs. 1 (a), (b) and (c) show the 0^- peak at a very similar excitation energy, while the values of NEWSR are somewhat different. The same is true for the 1^- peak in the three results. For the SLy4 interaction in Fig. 1(d), the 0^- and 1^- peaks appear at about 3 MeV lower than the other three results, having 76% and 68% of the NEWSR, respectively. This is due to the negative

TABLE III: Peak energies and the average energies of charge exchange SD excitations in the A=90 nuclei obtained by the self-consistent HF+RPA calculations: t_- in ^{90}Nb and t_+ in ^{90}Y . The average energy is calculated by the ratio of EWSR to NEWSR: $\bar{E}(\text{MeV})=m_1/m_0$. See the text for details.

	t_-		t_+	
	$E_{peak}(\text{MeV})$	$\bar{E}(\text{MeV})$	$E_{peak}(\text{MeV})$	$\bar{E}(\text{MeV})$
SIII	28.5	25.7	13.5	10.9
SGII	27.7	26.7	11.7	9.47
SkI3	29.3	28.2	12.8	11.6
SLy4	26.1	24.9	11.4	10.5

value of the Landau parameter G'_0 in SLy4 for the spin-isospin channel. The dominant configurations of the collective 0^- and 1^- states are the $(\pi 1h_{9/2}\nu 1g_{9/2}^{-1})$ and $(\pi 1g_{7/2}\nu 1f_{7/2}^{-1})$ configurations. For the 2^- excitations, the number of p-h configurations is larger than those of 0^- and 1^- and therefore the strength is fragmented in a wider energy range compared with 0^- and 1^- excitations. There is a small low-lying peak with $J^\pi = 2^-$ at $E_x = 12.4$ (14.1) MeV with 10.0 (9.0)% of the NEWSR value in the case of the SIII (SGII) interaction. This state is mainly due to the $\pi 1g_{9/2}\nu 1f_{5/2}^{-1}$ configuration. The major strengths are found in the two peaks around 21 and 27 MeV in both the SIII and SGII results. The strength around $E_x = 21$ MeV exhausts 50(41)% of the NEWSR value, while the peak around $E_x = 27$ MeV exhausts 30(37)% of the NEWSR value for the SIII (SGII) interaction. The peak energies in the two results are similar, while more SD strength is shifted to the peak around $E_x = 21$ MeV in the case of the SIII interaction. The main configurations of the higher peak at $E_x = 27$ MeV are the same as those of the 0^- and 1^- peaks, namely, $(\pi 1h_{9/2}\nu 1g_{9/2}^{-1})$ and $(\pi 1g_{7/2}\nu 1f_{7/2}^{-1})$. On the other hand, the main configurations of the peak around $E_x = 21$ MeV are $(\pi 1h_{11/2}\nu 1g_{9/2}^{-1})$, $(\pi 2d_{5/2}\nu 2p_{1/2}^{-1})$ and $(\pi 2d_{5/2}\nu 2p_{3/2}^{-1})$. The 2^- strength distributions of the SkI3 and SLy4 interactions are somewhat different than those of the SIII and SGII interactions. There is no isolated low energy peak in the results for the SkI3 and SLy4 interactions. Three large peaks are seen at $E_x = 23.5$, 26.5 and 29.5 MeV together with several small peaks, while the two peaks at 20 and 26 MeV exhaust most of the strengths in the case of SLy4.

The SD strengths calculated by the SD operator $\hat{S}_+^\lambda = \sum_i t_+^i r_i [\sigma \times Y_1(\hat{r}_i)]^\lambda$ are shown in

Fig. 2 (a), (b), (c) and (d) for the SIII, SGII, SkI3 and SLy4 interactions, respectively. The strength distributions are divided into two energy regions: a broad bump below 10 MeV and a peak around $E_x = 13$ MeV. The strengths below 10 MeV are due to the $\lambda^\pi=1^-$ and 2^- states, while the high energy peak is induced mainly by the 1^- states. The large 0^- strength is also found just above the high energy 1^- peak. The summed NEWSR values of all multipoles below 10 MeV are almost equal to the strength of the high energy peak around $E_x = 13$ MeV in the case of the SIII and SGII interactions. The high energy peak of the SIII interaction in Fig. 2(a) is about 2 MeV higher than those of SGII and SLy4, as listed in Table III. The main configuration for the high energy peaks with $\lambda^\pi=0^-$ 1^- and 2^- is the $(\nu 1g_{7/2}\pi 1f_{7/2}^{-1})$ excitation. For the low energy 1^- strength, the $(\nu 2d_{3/2}\pi 2p_{3/2}^{-1})$ and $(\nu 1g_{7/2}\pi 1f_{5/2}^{-1})$ configurations play the dominant roles. The $(\nu 2d_{5/2}\pi 2p_{1/2}^{-1})$, $(\nu 2d_{5/2}\pi 2p_{3/2}^{-1})$ and $(\nu 3s_{1/2}\pi 2p_{3/2}^{-1})$ configurations have a large contribution in the low energy peak of $\lambda^\pi = 2^-$. The $(\nu 2d_{3/2}\pi 1f_{7/2}^{-1})$ configuration contributes substantially to the high energy 2^- peak together with the $(\nu 1g_{7/2}\pi 1f_{7/2}^{-1})$ configuration. The large spread in the distributions of the SD strengths in Figs. 1 and 2 are due to the fact that the $p-h$ excitations are very different in unperturbed energy. Thus, the collision-less Landau damping effect plays an important role in the large observed width of SD resonance, while the coupling to the continuum plays a minor role. The coupling to 2-particle-2-hole (2p-2h) states were shown to increase substantially the width of the main peak of the t_- SD excitations of ^{90}Zr in ref. [28].

The energies of the main peaks E_{peak} are tabulated in Table III along with the average excitation energies, which are calculated by the ratio of the energy-weighted sum rule (EWSR) m_1 to the non-energy weighted sum rule (NEWSR) m_0 , $\bar{E} = m_1/m_0$. The \bar{E} is always lower than the E_{peak} because of the low energy peak in the excitation spectra. For the t_- response, the SkI3 interaction gives the highest excitation energy for the peak, while the SLy4 is the lowest. Notice that the energy of SkI3 is the highest due to the small effective mass m^*/m , while the negative Landau parameter G'_0 is responsible for the fact that SLy4 yields the lowest energy value in Table III. The general trend of the average excitation energy \bar{E} is the same for the t_+ response. The SIII, however, gives a somewhat higher energy for the E_{peak} than SkI3 does.

The calculated results of SD strength are shown in Fig. 3 together with the experimentally obtained distributions of the SD strengths [16]. The spectra for the t_+ channel are shifted by +23.6 MeV, accounting for the Coulomb energy difference between the daughter nuclei

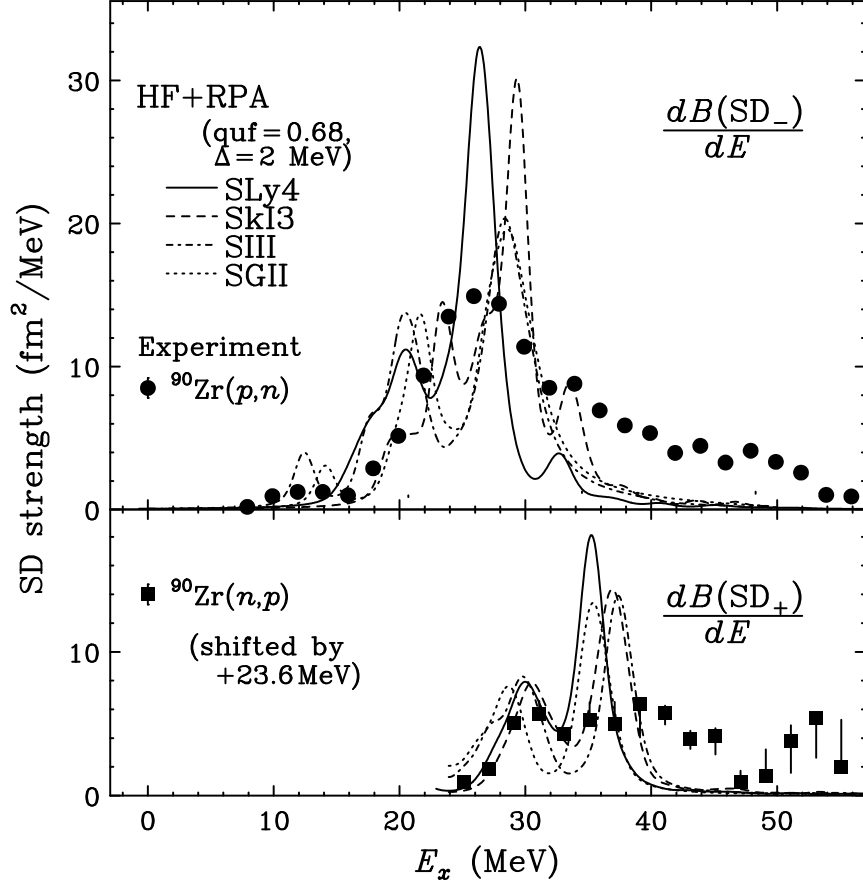


FIG. 3: Charge exchange SD strength $\frac{dB(SD_-)}{dE}$ (upper panel) and $\frac{dB(SD_+)}{dE}$ (lower panel) of ^{90}Zr . The circles and squares are the experimental data taken from ref. [16]. The spectra $\frac{dB(SD_+)}{dE}$ are shifted by the Coulomb energy difference between the two daughter nuclei ^{90}Nb and ^{90}Y (+23.6 MeV) to adjust the isospin difference between the two nuclei. The calculated results are plotted with the quenching factor $\text{quf} = 0.68$. The SD strength is averaged by the weighting function (5) with the width $\Delta = 2$ MeV.

^{90}Nb and ^{90}Yb . We introduce the quenching factor $\text{quf} = 0.68$ for both the t_- and t_+ channels. For the t_- channel, the experimental strength distribution peaked at $E_x \sim 26$ MeV is well described by the SLy4 interaction. The results of SGII and SIII also give reasonable agreement with the experimental peak energy. None of the calculated results show any substantial strength above $E_x \sim 36$ MeV, while a significant portion of the sum rule value is found above $E_x \sim 36$ MeV in the experimental data. This difference may be due to the lack of coupling to many-particle many-hole states in the present RPA calculations. In ref. [28], the t_- SD strengths in ^{90}Zr have been studied using the RPA model including

the couplings to 2p-2h states. It was found that the mixing between 1p-1h and 2p-2h states gives a large asymmetric spread in the strength of the SD resonances, and about 30% of the total strength is shifted to excitation energies above 35 MeV, referred to the parent nucleus ^{90}Zr . This result is consistent with the quenching factor adopted in Fig. 3. It should be mentioned that the peak energy of the t_- SD strength is not changed appreciably by the coupling to the 2p-2h states, while the peak height is decreased substantially.

For the t_+ channel, the two peak structures can be seen in both the calculated and experimental results. SkI3 and SLy4 describe the SD strength well at the low energy spectra. The calculated strength up to $E_x = 40$ MeV exhausts 100% of the sum rule value, while the experimental data show appreciable strength above $E_x = 40$ MeV. This difference may be due to the couplings to many-particle many-hole states similar to the t_- channel.

Let us now discuss the integrated SD strength. The integrated SD strength

$$m_0(E_x) = \sum_{\lambda^\pi=0^-,1^-,2^-} \int_0^{E_x} \frac{dB(\lambda)}{dE'} dE' \quad (6)$$

is plotted as a function of the excitation energy E_x in Fig. 4 for the operators $\hat{S}_-^\lambda = \sum_i t_-^i r_i [\sigma \times Y_1(\hat{r}_i)]^\lambda$ and $\hat{S}_+^\lambda = \sum_i t_+^i r_i [\sigma \times Y_1(\hat{r}_i)]^\lambda$. The experimental data are taken from ref. [16]. The value S_- is obtained by integrating up to $E_x = 50$ MeV from the ground state of the daughter nucleus ^{90}Nb ($E_x = 57$ MeV from the ground state of the parent nucleus ^{90}Zr), while the corresponding value S_+ is evaluated up to $E_x = 26$ MeV from the ground state of ^{90}Y ($E_x = 27.5$ MeV from the ground state of the ^{90}Zr). This difference between the two maximum energies of the integrals stems from the isospin difference between the ground states of the daughter nuclei, i.e., $T=4$ in ^{90}Nb and $T=6$ in ^{90}Y . That is, the 23.6 MeV difference originates from the difference in excitation energy between the $T=6$ Gamow-Teller states in the (p,n) and (n,p) channels[16]. For both the S_- and S_+ strength, the calculated results overshoot the experimental data in the energy range $E_x = 20$ -40 MeV. These results suggest the quenching of 30-40% of the calculated strength around the peak region, as was already mentioned. However, the integrated cross-sections up to $E_x = 56$ MeV in Fig. 4 approach the calculated values for both the t_- and t_+ channels.

The calculated SD sum rule values in $A=90$ nuclei obtained by using the HF+RPA results are tabulated in Table IV for the transitions with $\lambda^\pi = 0^-, 1^-$ and 2^- . Clearly, the ΔS values show signs of multipole proportionality ($2\lambda+1$), even though S_- and S_+ themselves do not show any clear multipole dependence. The present RPA results for ^{90}Zr listed in Table IV

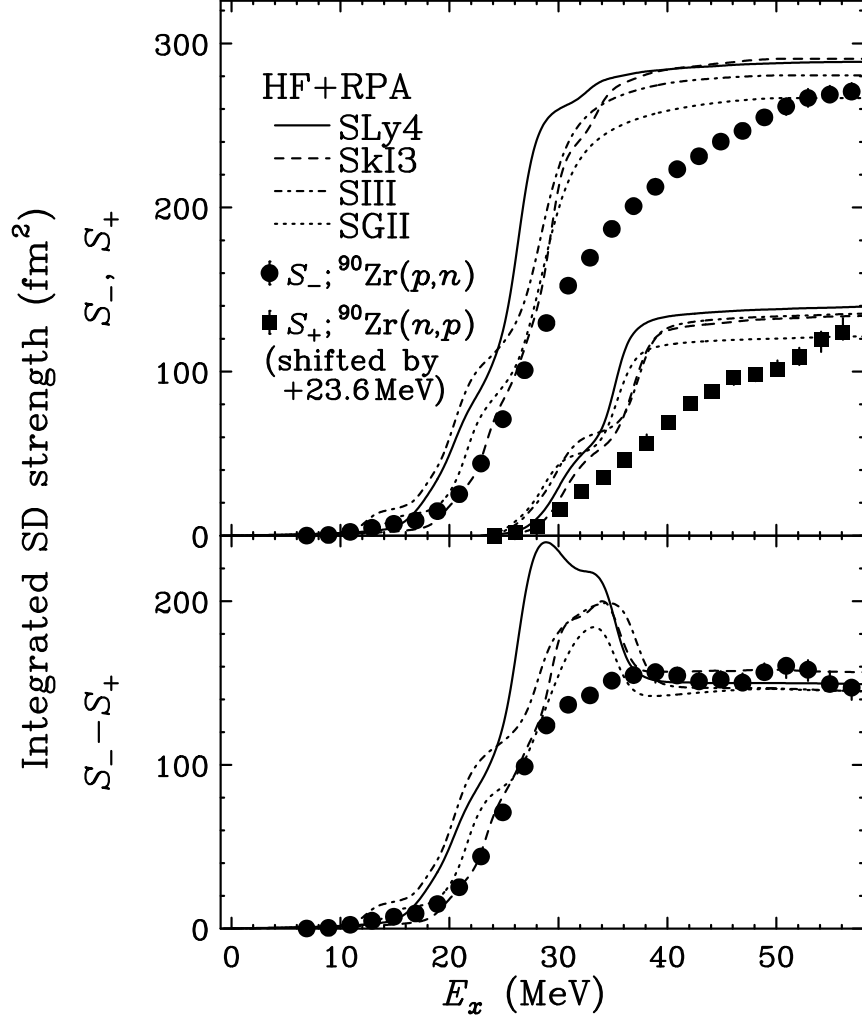


FIG. 4: Integrated charge exchange SD strength (6) excited by the operators $\hat{S}_- = \sum_{i,m,\mu} t_-^i \sigma_m^i r_i Y_1^\mu(\hat{r}_i)$ and $\hat{S}_+ = \sum_{i,m,\mu} t_+^i \sigma_m^i r_i Y_1^\mu(\hat{r}_i)$ on ^{90}Zr . The calculated results are obtained by the HF+RPA model using the Skyrme interactions SIII, SGII, SLy4 and SkI3. The upper panel shows the S_- and S_+ strength, while the lower panel shows the $S_- - S_+$ strength. All strengths for the three multipoles $\lambda^\pi=0^-, 1^-, 2^-$ are summed up in the results. The experimental data are taken from ref. [16]. No quenching factor is introduced in the calculation of the integrated strength.

satisfy the sum rule value (2) in Table II with high accuracy, to an error of only (0.1~0.2)%. This agreement guarantees the numerical accuracy of the present RPA calculations. This is also the case in ^{208}Pb , as will be shown in Section IIB. The $\Delta S = S_- - S_+$ value is shown as a function of E_x in the lower panel of Fig. 4. We note that the ΔS value saturates both in

TABLE IV: Sum rule values of charge exchange SD excitations in A=90 nuclei obtained by the HF+RPA calculations; S_- for ^{90}Nb and S_+ for ^{90}Y . The SD strength is integrated up to $E_x = 50$ MeV for S_- and $E_x = 26$ MeV for S_+ , respectively. The experimental data are taken from ref. [16]. The SD sum rules are given in units of fm^2 . See the text for details.

	SIII			SGII			SkI3			SLy4		
λ^π	S_-	S_+	ΔS	S_-	S_+	ΔS	S_-	S_+	ΔS	S_-	S_+	ΔS
0^-	34.8	18.5	16.4	33.2	17.4	15.8	36.6	19.1	17.5	37.8	21.4	16.4
1^-	120.8	71.7	49.1	122.0	74.3	47.7	120.8	68.2	52.7	115.8	66.4	49.4
2^-	130.1	48.5	81.6	125.5	45.9	79.5	139.0	51.1	87.9	138.7	56.4	82.3
sum	285.7	138.6	147.1	280.7	137.6	143.1	296.3	138.3	158.1	292.3	144.2	148.2
exp	$S_- = 271 \pm 14$			$S_+ = 124 \pm 11$			$\Delta S = 147 \pm 13$					

the calculated and the experimental values above $E_x = 40$ MeV, while the empirical values S_- and S_+ themselves increase gradually above $E_x = 40$ MeV. This is the crucial feature for extracting the model-independent sum rule $\Delta S = S_- - S_+$ from the experimental data. The empirical values S_- , S_+ and ΔS obtained from these analyses are shown in Table IV. The indicated uncertainties of S_- , S_+ and ΔS contain not only the statistical error of the data, but also errors due to the various input of the DWIA calculations used in the MD analysis, such as, the optical model parameters and the single-particle potentials [15]. There is an additional uncertainty in the estimation of the SD unit cross-section, namely, the overall normalization factor [16], which should be studied further experimentally.

From ΔS , the neutron radius of ^{90}Zr is extracted to be $\sqrt{\langle r^2 \rangle_n} = (4.26 \pm 0.04)\text{fm}$ from the model-independent SD sum rule (3), where the empirical proton radius $\sqrt{\langle r^2 \rangle_p} = 4.19$ fm is used. The proton radius is obtained from the charge radius in Table II by subtracting the proton finite size correction. The experimental uncertainty in the neutron skin thickness obtained by proton scattering is rather large: $\delta_{np} = r_n - r_p = (0.09 \pm 0.07)\text{fm}$. This is because of the model-dependent analysis of the proton scattering, with effective nucleon-nucleon interactions in the nuclei [7]. On the other hand, the sum rule analysis of the SD strength determines the neutron radius with 1% accuracy, which is almost the same as that expected for the parity violation electron scattering experiment. The obtained value $r_n - r_p = (0.07 \pm 0.04)$ fm can be used to disentangle the neutron matter EOS by using the

strong linear correlation between the two quantities [1, 2, 3], as will be discussed in Section 3.

B. Charge exchange SD excitations of ^{208}Pb

TABLE V: Proton, neutron and charge radii of ^{208}Pb . The charge radius is obtained by folding the proton finite size. The sum rule values $\Delta S = S_- - S_+$ of the SD excitations are calculated by Eq. (3) with the HF neutron and proton mean square radii. Experimental data on the charge radius are taken from ref. [27]. Experimental data on $\delta_{np} = r_n - r_p$ are obtained by the proton scattering [8, 9, 10] and the giant dipole excitations of ^{208}Pb [11]. The radii are given in units of fm, while the SD sum rules are given in units of fm².

	SIII	SGII	SkI3	SLy4	exp
r_p	5.521	5.454	5.421	5.457	—
r_c	5.578	5.512	5.479	5.515	5.503 ± 0.002
r_n	5.646	5.589	5.649	5.617	—
$\delta_{np} = r_n - r_p$	0.125	0.135	0.228	0.160	$0.083 < \delta_{np} < 0.111$ [8], 0.19 ± 0.09 [11]
ΔS	1086.	1072.	1154.	1098.	

The HF results of ^{208}Pb are summarized in Table V. The RPA results of SD excitations of ^{208}Pb are given in Figs. 5 and 6 for the four different Skyrme interactions, namely, SIII, SGII, SkI3, and SLy4. For the t_- channel, the strength distributions are spread out in a broad energy region ($15 \text{ MeV} < E_x < 35 \text{ MeV}$) except a tiny peak at $E_x \sim 5 \text{ MeV}$. On the other hand, the strength for the t_+ channel is concentrated in a single narrow peak. The highest peak of the t_- channel occurs at $E_x \sim 27\text{-}28 \text{ MeV}$ in the cases of the SIII, SGII, and SLy4 interactions, while it is shifted to higher energies ($E_x \sim 33 \text{ MeV}$) in the case of SkI3. The 0^- and 1^- excitations have merged into one peak, having more than 40% of the total strength at the high energy side, while the 2^- states split into a broad energy region. The low-energy 2^- state at around $E_x = 4 \text{ MeV}$ is mainly due to the $(\pi 1h_{9/2}\nu 1i_{13/2}^{-1})$ excitation. The 0^- peak is predicted to occur at a slightly higher energy than the 1^- peak. However, it might be difficult to observe this peak experimentally because of its rather low strength. There are appreciable differences in the peak energies between the Skyrme interactions for

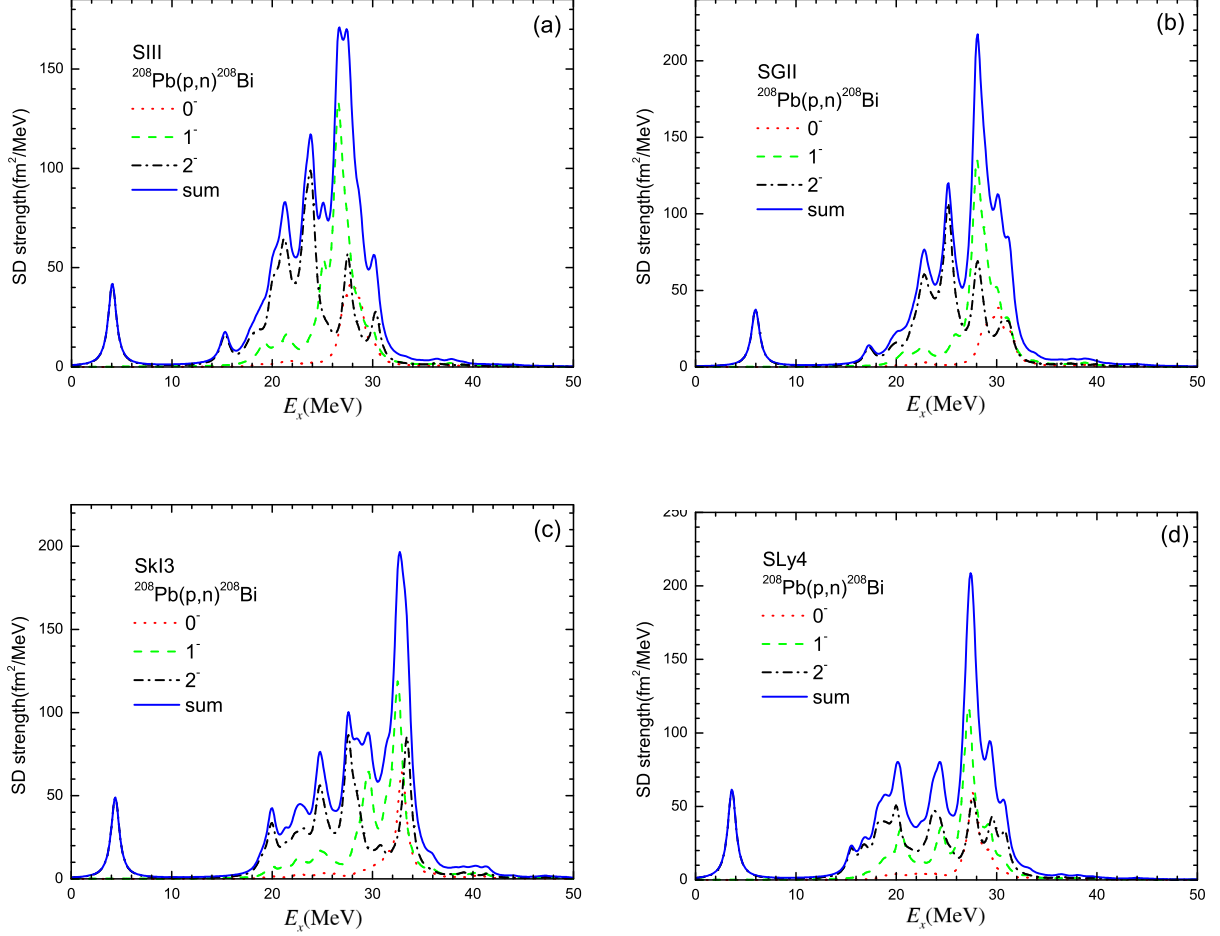


FIG. 5: (Color online) Charge exchange SD strengths for the operators $\hat{S}_-^\lambda = \sum_i t_-^i r_i [\sigma \times Y_1(\hat{r}_i)]^\lambda$ calculated by the HF+RPA model with the Skyrme interactions (a) SIII, (b) SGII, (c) SkI3, and (d) SLy4. The excitation energy is referred to the ground state of the parent nucleus ^{208}Pb . The SD strength is averaged by the weighting function in Eq. (5) with the width $\Delta = 1$ MeV.

the t_+ channel: $E_x \sim 3$ MeV for SGII, $E_x \sim 5$ MeV for SIII and $E_x \sim 6$ MeV for SLy4 and SkI3, as listed in Table VI. The sum rule values S_- and S_+ are listed in Table VII. Because of the strong Pauli blocking of neutron excess in ^{208}Pb , the S_+ value is much smaller than the S_- value, at most, 20% of the corresponding S_- value for each multipole. The S_+ value is substantial in the case of $A=90$ as shown in Table IV, more than 55% of S_- in some cases. However, $\Delta S = S_- - S_+$ obeys the $(2\lambda+1)$ proportionality, as expected from Eq. (2). The charge exchange $^{208}\text{Pb}(^3\text{He}, t)^{208}\text{Bi}$ reaction was performed to study the SD strength in ^{208}Bi . The data were analyzed by a least-squares fitting method and the peak of the SD strength was found to be at $E_x = 24.8 \pm 0.8$ MeV, as measured from the ground state of ^{208}Pb [29].

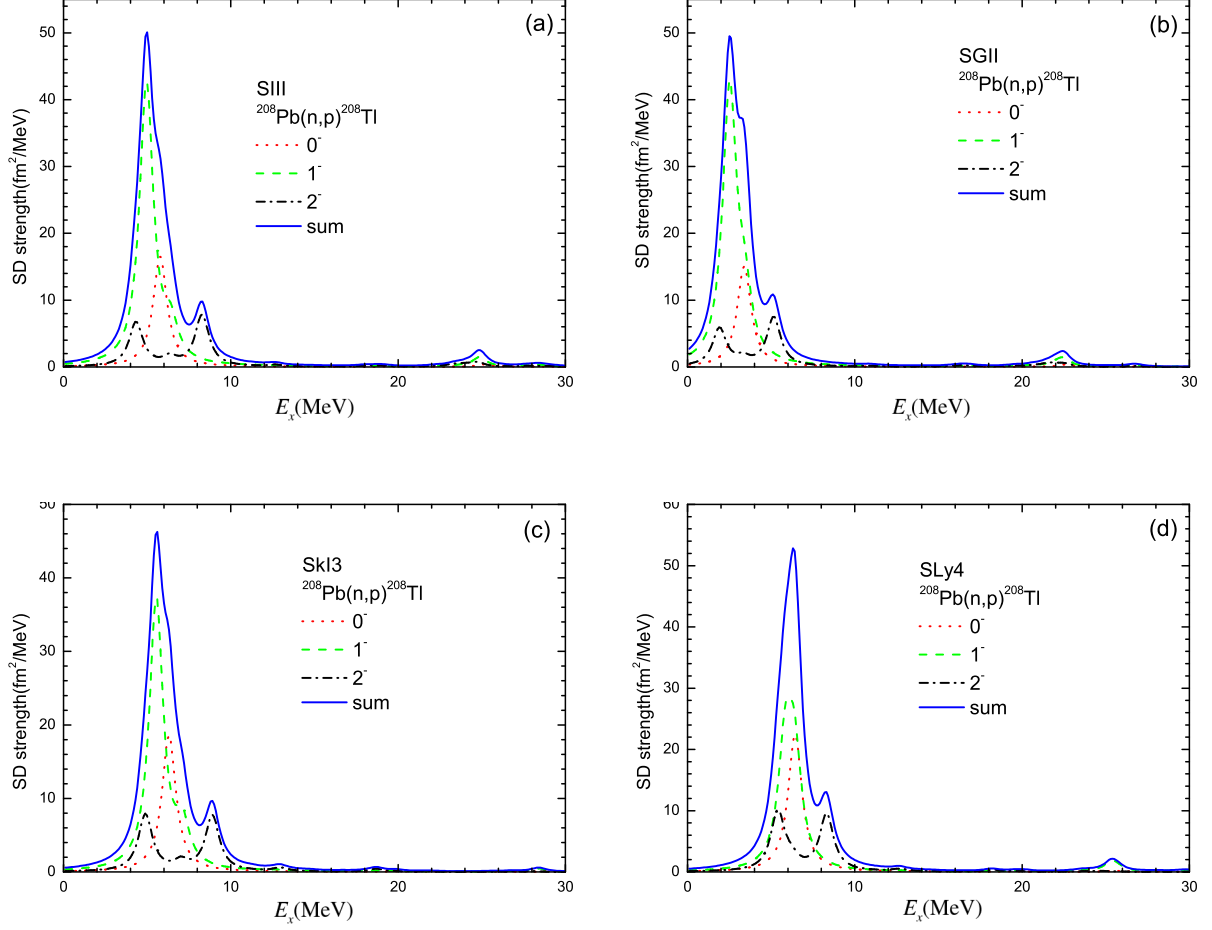


FIG. 6: (Color online) Charge exchange SD strengths for the operators $\hat{S}_+^\lambda = \sum_i t_+^i r_i [\sigma \times Y_1(\hat{r}_i)]^\lambda$ calculated by the HF+RPA model with the Skyrme interactions (a) SIII, (b) SGII, (c) SkI3 and (d) SLy4. The excitation energy is referred to the ground state of the parent nucleus ^{208}Pb . The SD strength is averaged by the weighting function in Eq. (5) with the width $\Delta = 1$ MeV.

This empirical peak energy is close to the average energy \bar{E} of SD strength obtained by SIII and SGII in Table VI. Further experimental effort is urgently needed to obtain more quantitative strength distributions, for example, for the multipole decomposition analysis of charge exchange reactions on a ^{208}Pb target.

One can see only one sharp peak in the t_+ channel in Fig. 6. There are only two allowed 1p-1h configurations ($\nu 2g_{9/2}\pi 1h_{11/2}^{-1}$) and ($\nu 1i_{11/2}\pi 1h_{11/2}^{-1}$) for both 1^- and 2^- excitations because of the strong Pauli blocking effect of excess neutrons. Moreover, the $\nu 2g_{9/2}$ and $\nu 1i_{11/2}$ states are almost degenerate in energy in the HF potential. They are the reasons why there is only one sharp peak in the t_+ channel of ^{208}Pb . It might be interesting to perform

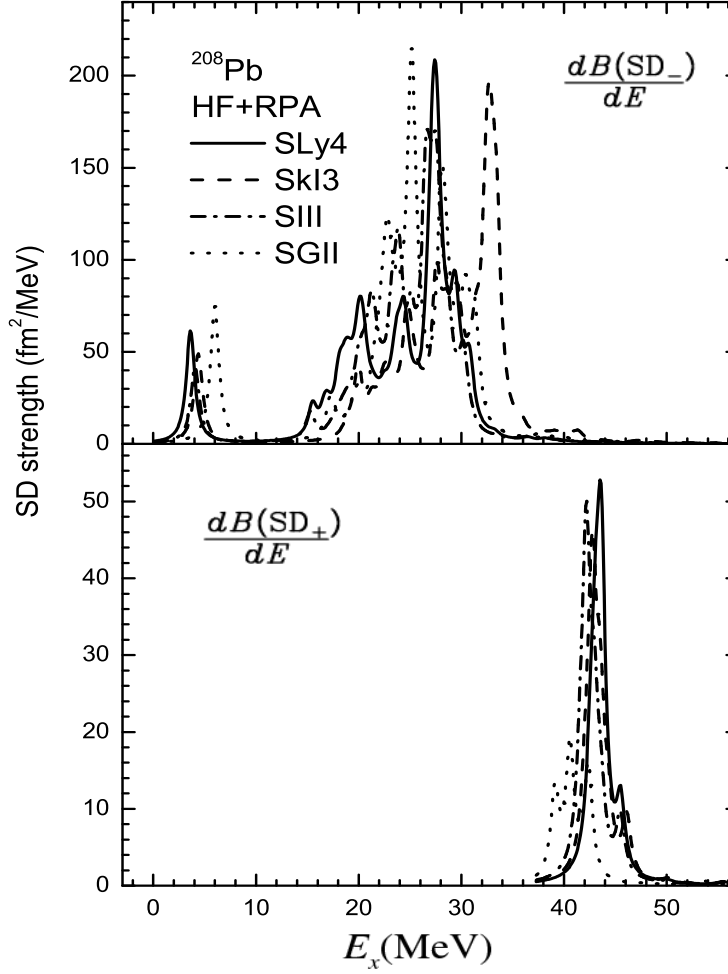


FIG. 7: Charge exchange SD strength $\frac{dB(SD_-)}{dE}$ (upper panel) and $\frac{dB(SD_+)}{dE}$ (lower panel) of ^{208}Pb . The spectra $\frac{dB(SD_+)}{dE}$ are shifted by +37.2 MeV due to the Coulomb energy difference between the two daughter nuclei ^{208}Bi and ^{208}Tl . The arrow in the upper panel shows a peak energy at $E_x = 24.8$ MeV observed by the charge exchange reaction $^{208}\text{Pb}(^3\text{He}, t)^{208}\text{Bi}$ [29].

$^{208}\text{Pb}(n, p)^{208}\text{Tl}$ or $^{208}\text{Pb}(t, ^3\text{He})^{208}\text{Tl}$ reactions in order to observe this peak experimentally. The $^{208}\text{Pb}(n, p)^{208}\text{Tl}$ reaction has been reported for the t_+ channel, and a broad peak found at $E_x \sim 8$ MeV, as measured from the ground state of ^{208}Pb with rather poor statistics [30].

The integrated SD strengths for both the t_- and t_+ channels are shown in Fig. 8. The calculated NEWSR shows a saturation at around $E_x \sim 30$ MeV as can be seen in Fig. 8. As noted previously, the t_+ channel has only a small contribution to the model-independent

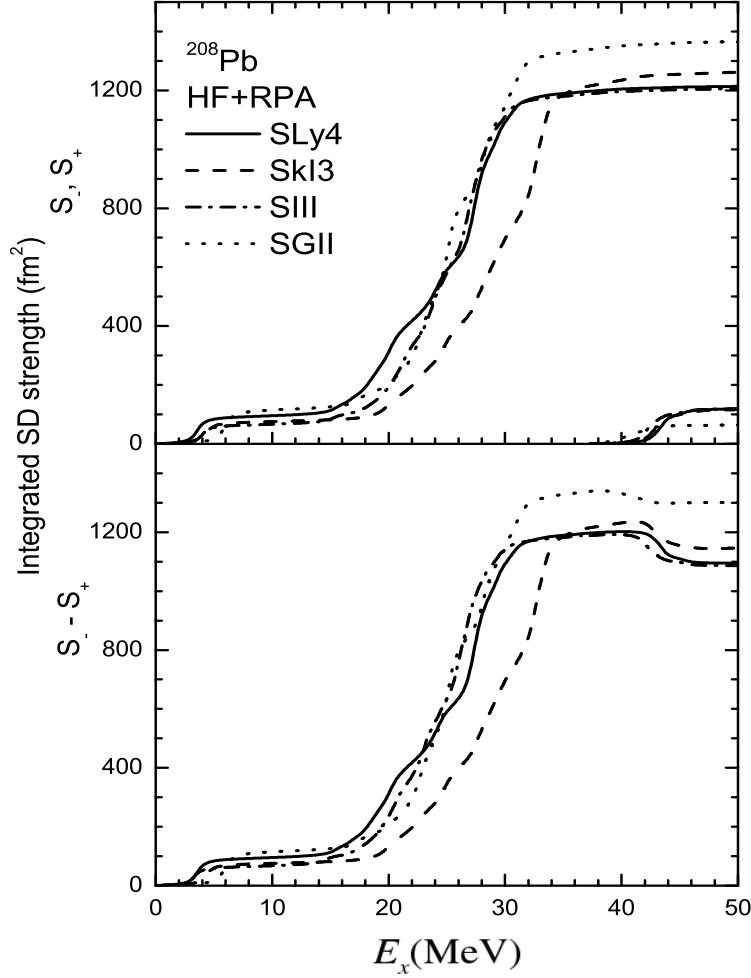


FIG. 8: Integrated charge exchange SD strength (6) of ^{208}Pb for the operators $\hat{S}_- = \sum_{i,m,\mu} t_-^i \sigma_m^i r_i Y_1^\mu(\hat{r}_i)$ and $\hat{S}_+ = \sum_{i,m,\mu} t_+^i \sigma_m^i r_i Y_1^\mu(\hat{r}_i)$ calculated by the HF+RPA model with the Skyrme interactions SIII, SGII, SkI3 and SLy4. The upper panel shows the S_- and S_+ strength, while the lower panel shows the $\Delta S = S_- - S_+$ strength. All strengths for the three multipoles $\lambda^\pi=0^-, 1^-$ and 2^- are summed up in the results.

sum rule ΔS .

The couplings to the 2p-2h states may increase the spread in the SD strength in $A=208$ nuclei as well as $A=90$ nuclei. So far, the charge exchange Gamow-Teller(GT) states in ^{208}Bi were studied by taking into account the couplings to 2p-2h states in the particle-vibration model [24]. While a large spread was found in the GT states in the particle-vibration model

TABLE VI: Peak energies and the average energies of charge exchange SD excitations in A=208 nuclei calculated by the HF+RPA model; S_- for ^{208}Bi and S_+ for ^{208}Tl . The average energy is calculated by the ratio of EWSR to NEWSR: $\bar{E}(\text{MeV})=m_1/m_0$. See the text for details

	t_-		t_+	
	$E_{peak}(\text{MeV})$	$\bar{E}(\text{MeV})$	$E_{peak}(\text{MeV})$	$\bar{E}(\text{MeV})$
SIH	26.7	24.2	5.0	7.3
SGII	28.1	24.6	2.5	6.0
SkI3	32.7	27.9	5.6	7.3
SLy4	27.4	23.6	6.3	8.0

TABLE VII: Sum rule values of charge exchange SD excitations in A=208 nuclei calculated by the HF+RPA model; S_- for ^{208}Bi and S_+ for ^{208}Tl . The SD strength is integrated up to $E_x = 57$ MeV for S_- and $E_x = 20$ MeV for S_+ ; the excitation energy is referred to the ground state of ^{208}Pb . The SD sum rules are given in units of fm^2 . See the text for details.

	SIH			SGII			SkI3			SLy4		
λ^π	S_-	S_+	ΔS	S_-	S_+	ΔS	S_-	S_+	ΔS	S_-	S_+	ΔS
0^-	148.6	27.0	121.6	114.1	24.3	119.8	158.0	29.7	128.3	158.5	36.0	122.5
1^-	442.7	78.8	363.9	440.4	82.3	358.1	454.5	69.2	385.3	430.8	63.6	367.2
2^-	632.2	28.3	603.9	620.7	26.4	595.3	669.8	28.2	641.6	644.5	34.1	610.5
sum	1224.	134.1	1089.	1205.	132.0	1073.	1282.	127.1	1155.	1234.	133.7	1100.

calculations, the peak energy did not change appreciably due to the couplings to 2p-2h states. There have been no microscopic studies of SD states that take into account the couplings to 2p-2h states in A=208 nuclei.

III. SD SUM RULES AND NEUTRON MATTER EOS

Sum rules are useful tools to study the collective nature of excitation modes in many-body systems. In particular, for charge exchange excitations, model-independent sum rules are derived and used to analyze experimental data on Gamow-Teller resonances and SD resonances [13]. For SD states, the sum rules can be used to extract the neutron skin thickness,

as was discussed in Section 2. References [1, 2, 3] have reported a strong correlation between the neutron skin thickness and the neutron matter EOS, as obtained by using Skyrme and relativistic mean field theories. In this section, we will study the relation between the SD sum rules and the neutron matter EOS. The strong linear correlation between the neutron skin thickness

$$\delta_{np} = \sqrt{\langle r^2 \rangle_n} - \sqrt{\langle r^2 \rangle_p} \quad (7)$$

and the pressure of neutron matter

$$P = \rho_n \frac{d(E(\rho_n)/\rho_n)}{d\rho_n}. \quad (8)$$

is essential for this study. Other linear correlations between the neutron skin thickness and various isovector nuclear matter properties have also been pointed out recently [6]. Given these correlations, accurate information on the neutron skin thickness will be quite useful in determining empirically the pressure of neutron matter EOS and isovector nuclear properties, such as the volume and surface symmetry energies.

The correlations between the pressure of neutron matter at the neutron density $\rho_n = 0.1 \text{ fm}^{-3}$ and the charge exchange SD sum rules of ^{90}Zr and ^{208}Pb are shown in Figs. 9 and 10 with 12 different Skyrme interactions. The numbers denote different Skyrme parameter sets: 1 for SI, 2 for SIII, 3 for SIV, 4 for SVI, 5 for Skya, 6 for SkM, 7 for SkM*, 8 for SLy4, 9 for MSkA, 10 for SkI3, 11 for SkX and 12 for SGII. The correlation coefficients from the extrapolated lines are $r = 0.888$ and 0.811 for ^{208}Pb and ^{90}Zr , respectively. The correlation coefficients are somewhat smaller than those of the calculated correlation between the neutron skin thickness δ_{np} and the pressure P in ref. [3], but still, we can see fairly good correlations in Figs. 9 and 10.

The rms proton, charge, and neutron radii in ^{90}Zr calculated by the HF model with the four interactions SIII, SGII, SkI3 and SLy4 are shown in Table II. The calculated charge radii of the SGII and SkI3 interactions show reasonable agreement with the experimental values. However, there is a factor 2 difference in the neutron skin thickness δ_{np} between the two interactions. As seen in Table II, the neutron skin thickness δ_{np} obtained by the SD sum rules is consistent with the value previously obtained from the proton scattering data. However, the experimental uncertainty in the value $\delta_{np} = (0.07 \pm 0.04) \text{ fm}$ obtained by the SD sum rules is half that obtained through the proton data. This small uncertainty will help

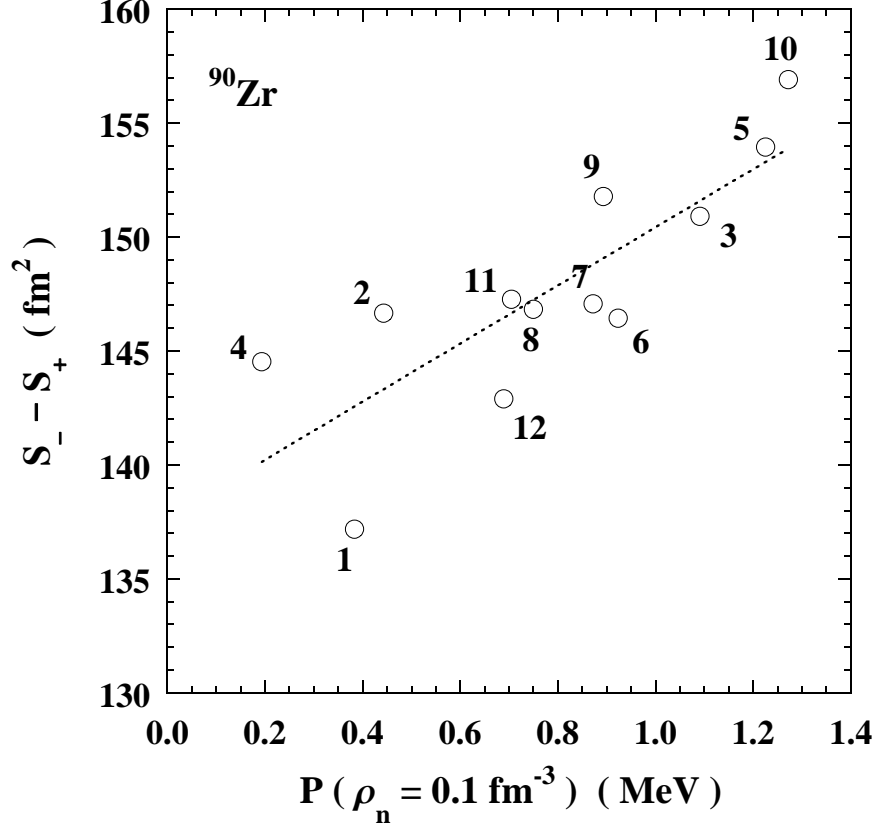


FIG. 9: Correlations between the pressure of neutron matter and the SD sum rule values of ^{90}Zr with 12 different Skyrme interactions. The numbers denote different Skyrme parameter sets: 1 for SI, 2 for SIII, 3 for SIV, 4 for SVI, 5 for Skya, 6 for SkM, 7 for SkM*, 8 for SLy4, 9 for MSkA, 10 for SkI3, 11 for SkX and 12 for SGII. The correlation coefficient is found to be $r = 0.811$.

to disentangle the neutron matter EOS using the strong correlation with the neutron skin thickness. The experimental skin thickness $\delta_{np} = 0.07 \pm 0.04 \text{ fm}$ is close to the HF results of SLy4, as well as SGII and SIII. The SkI3 result is not favored over the empirical result, even taking the experimental uncertainties into consideration. We should also note that the experimental peak energy of t_- SD strength in ^{90}Nb coincides with the calculated peak energy of the SLy4 interaction, while that of SkI3 is 4 MeV above the experimental value, as seen in Fig. 3. While all interactions lie within the experimental value $\Delta S = (147 \pm 13) \text{ fm}^2$ in Fig. 9, the empirical data favor the interactions indicated by the numbers 2(SIII), 11(SkX), 8(SLy4), 7(SkM*) and 6(SkM). These interactions suggest a soft neutron matter EOS with the pressure $P(\rho_n=0.1 \text{ fm}^{-3}) = (0.65 \pm 0.2) \text{ MeV}$. Thus, the preferred nuclear matter symmetry energy extracted from the SD experiment is found to be $J = (30 \pm 2) \text{ MeV}$ as a result of

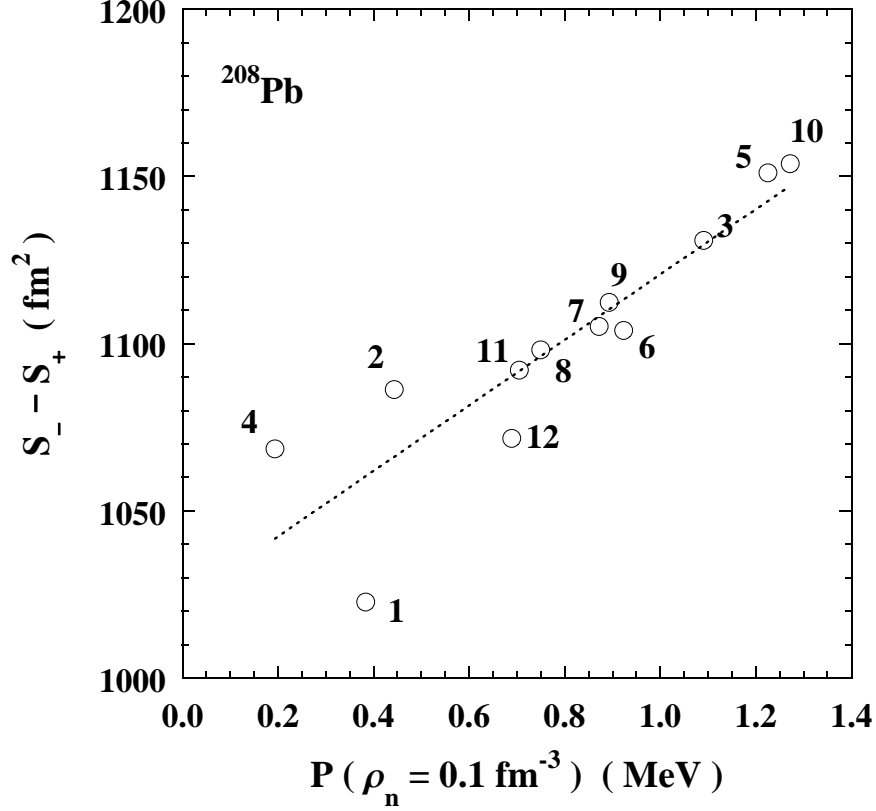


FIG. 10: Correlations between the pressure of neutron matter and the SD sum rule values of ^{208}Pb with 12 different Skyrme interactions. The numbers denote different Skyrme parameter sets: 1 for SI, 2 for SIII, 3 for SIV, 4 for SVI, 5 for Skya, 6 for SkM, 7 for SkM*, 8 for SLy4, 9 for MSkA, 10 for SkI3, 11 for SkX and 12 for SGII. The dashed line represents the result obtained by the least-squares method. The correlation coefficient is found to be $r = 0.888$.

the strong correlation between the neutron skin thickness and the symmetry energy [2, 5].

Table V tabulates the rms proton, charge and neutron radii in ^{208}Pb calculated by the HF model, along with the experimental charge radius. The HF results of SGII and SLy4 account for the experimental charge radius, while there is a large variation in the predictions for the neutron skin thickness δ_{np} . The empirical value of the neutron skin thickness δ_{np} in ^{208}Pb was obtained by proton scattering experiments. However, the values obtained depend very much on the experiments and analyses. That is, the experimental errors are still large and some of the values obtained have no overlap, even when the uncertainty in the analyses is taken into account; $\delta_{np} = (0.14 \pm 0.02)$ fm in ref. [9], $\delta_{np} = (0.20 \pm 0.04)$ fm in ref. [10] and $(0.083 < \delta_{np} < 0.111)$ fm in ref. [8]. We quote in Table V the value

in ref. [8] where the analyses were performed comprehensively with many different sets of data including those adopted in refs. [9, 10]. Although these results depend on the effective nucleon-nucleon effective interactions in nuclei used in the analysis, the comprehensive study of proton scattering in ref. [8] reports rather small neutron skin thicknesses, even smaller than the smallest value in Table V obtained using the SIII interaction. Again, this small δ_{np} suggests a soft neutron matter EOS similar to the conclusion reached by the SD sum rules of ^{90}Zr . The charge exchange $^{208}\text{Pb}(^3\text{He},t)^{208}\text{Bi}$ reaction data [29] show an SD peak in ^{208}Bi at $E_x = 24.8 \pm 0.8$ MeV measured from the ground state of ^{208}Pb , as marked by an arrow in Fig. 7. This peak position is close to the calculated value of the SGII interaction, while the SkI3 peak is a few MeV higher than the empirical value. This comparison may exclude the prediction by SkI3, which gives a hard neutron matter EOS in Fig. 10 marked by the number 10.

The neutron skin thickness was determined by the giant dipole resonance experiment to be $\delta_{np} = (0.19 \pm 0.09)\text{fm}$ [11]. This analysis depends on the adopted transition density and also the optical potentials so that the result is highly model-dependent. We definitely need more quantitative information, i.e., model-independent information on the neutron skin thickness in ^{208}Pb for precise determination of the neutron matter EOS as well as the isovector nuclear matter properties. To this end, the charge exchange SD experiments of ^{208}Pb will provide useful model-independent information with the same accuracy as the parity violation electron scattering experiment.

IV. SUMMARY

We have investigated the SD excitations in ^{90}Zr and ^{208}Pb using the HF + RPA model with four Skyrme interactions, viz., SIII, SGII, SkI3 and SLy4. It is shown that the Landau damping effect plays an important role in explaining the large observed width of SD resonance, while the coupling to the continuum is rather weak. Among the four interactions, the peak position of the experimental t_- SD strength in ^{90}Nb is well described by the SLy4 interaction, while the results of SIII and SGII are also acceptable. For the t_+ excitation of ^{90}Zr , a two-peak structure was found in both the experimental and calculated results. The SLy4 and SkI3 results showed good agreement with the observed low energy peak. We pointed out that the calculated results need a quenching factor $\text{quf} \simeq 0.68$ to al-

low a quantitative comparison with the experimental data up to $E_x = 36(40)$ MeV for the $t_-(t_+)$ channel in Fig. 3. About 30% of the NEWSR value is found in the excitation energy above $E_x = 36(40)$ MeV for the $^{90}\text{Zr}(p,n) ^{90}\text{Nb}$ ($^{90}\text{Zr}(n,p) ^{90}\text{Y}$) experiments. The calculated SD sum rule $\Delta S = S_- - S_+$ shows good saturation properties above $E_x = 40$ MeV without any quenching factor relative to the observed data despite the fact that sum rules S_- and S_+ themselves increase gradually above $E_x \geq 40$ MeV. The neutron skin thickness $\delta_{np} = 0.07 \pm 0.04$ fm extracted from the SD sum rules is close to the calculated values obtained using SLy4 as well as SIII and SGII. However, the extracted value does not favor the SkI3 interaction which gives almost twice as large a neutron skin thickness as SIII and SGII. This is indicative of the soft neutron matter EOS induced by the strong linear correlation between the neutron matter EOS and the neutron skin thickness. We showed that the SD strength of the t_- excitation of ^{208}Pb has a large width due to the Landau damping effect. In contrast, the t_+ excitation of ^{208}Pb turns out to be a single peak in a rather low energy region because of the strong Pauli blocking effect of the excess neutrons. The peak of the t_- SD strength was observed by $^{208}\text{Pb}(^3\text{He},t) ^{208}\text{Bi}$ at $E_x \sim 25$ MeV. This peak energy coincides with the peak calculated using the SGII interaction, while the SkI3 interaction yields a peak that is a few MeV higher than the empirical peak. Thus, the empirical SD sum rule values of ^{90}Zr and the observed peak energies of the t_- SD strength distributions in ^{90}Nb and ^{208}Bi indicate a soft neutron matter EOS with a pressure of $P(\rho_n=0.1\text{fm}^{-3}) = (0.65 \pm 0.2)$ MeV. The nuclear matter symmetry energy is also determined to be $J = (30 \pm 2)$ MeV from the strong correlation between the neutron skin thickness and the symmetry energy. In order to draw a more definite conclusion on the SD sum rules, as well as the neutron skin thickness and the neutron matter EOS, we need quantitative experimental work to obtain the SD sum rules in heavy nuclei like ^{208}Pb , both in the t_- and t_+ channels.

Acknowledgments

The authors would like express their thanks to I. Hamamoto for useful discussions. This work was supported in part by Grant-in-Aid for Scientific Research No. 16540259 and No. 17002003 from the Ministry of Education, Science, Culture and Sports and National Natural

- [1] B. A. Brown, Phys. Rev. Lett. **85**, 5296 (2000).
S. Typel and B. A. Brown, Phys. Rev. C**64**, 027302 (2001).
- [2] R. J. Furnstahl, Nucl. Phys. **A706**, 85 (2002).
- [3] S. Yoshida and H. Sagawa, Phys. Rev. C**69**, 024318(2004).
- [4] J. M. Lattimer and M. Prakash, Science **304**, 536 (2004).
A. W. Steiner, M. Prakash, J. M. Lattimer and P. J. Ellis, Phys. Report **411**, 335 (2005).
- [5] P. Danielewicz, Nucl. Phys. **A727**, 233(2003).
- [6] S. Yoshida and H. Sagawa, Phys. Rev. C**73**, 044320 (2006).
- [7] L. Ray, G. W. Hoffman , G. S. Blanpied, W. R. Coker and R. P. Liljestrand, Phys. Rev. C**18**, 1756 (1978).
L. Ray, G. W. Hoffman and W. R. Coker, Phys. Report **212**, 223 (1992).
- [8] R. C. Clark, L. J. Kerr and S. Hama, Phys. Rev. C**67**, 054605 (2003).
- [9] G. W. Hoffman, *etal*, Phys. Rev. C**21**, 1488 (1980).
- [10] V. E. Starodubsky and N. M. Hintz, Phys. Rev. C**49**, 2118 (1994).
- [11] A. Krasznahorkay et al., Phys. Rev. Lett. **66**, 1287 (1991); Nucl. Phys. **A567**, 521 (1994).
- [12] C. J. Horowitz, S. J. Pollock, P. A. Souder and R. Michaels, Phys. Rev. C**63**, 025501 (2001).
- [13] C. Gaarde et al., Nucl. Phys. **A369**, 258 (1981).
- [14] T. Wakasa, H. Sakai, H. Okamura, H. Otsu, S. Fujita, S. Ishida, N. Sakamoto, T. Uesaka, and
Y. Satou, M. B. Greenfield and K. Hatanaka, Phys. Rev. C**55**, 2909(1997).
- [15] K. Yako et al., Phys. Lett. **B615**, 193(2005).
- [16] K. Yako, H. Sagawa and H. Sakai, Phys. Rev. C**74** ,051303(R) (2006).
- [17] M. Ichimura, H. Sakai and T. Wakasa, Prog. Part. and Nucl. Phys. 56, 446 (2006).
- [18] A. Krasznahorkay et al., Phys. Rev. Lett. **82**, 3216(1999).
- [19] E. Kolbe and K. Langanke, Phys. Rev. C**63**, 025802 (2001);
T. Suzuki and H. Sagawa, Nucl. Phys. A718, 446c (2003).
- [20] G. F. Bertsch and S. F. Tsai, Phys. Report **18**, 125 (1975) ;
K. F. Liu and G. E. Brown, Nucl. Phys. **A265**, 385 (1976);
K. F. Liu and Nguyen Van Giai, Phys. Lett. **65B**, 23 (1976).

- [21] I. Hamamoto, H. Sagawa and X. Z. Zhang, Phys. Rev. **C55**, 2361 (1997).
- [22] Nguyen Van Giai and H. Sagawa, Phys. Lett. **B106**, 379 (1981).
- [23] M. Beiner, H. Flocard, Nguyen Van Giai and P. Quentin, Nucl. Phys. **A238**, 29 (1975).
- [24] G. Colò, Nguyen Van Giai, P. F. Bortignon and R. A. Broglia, Phys. Rev. **C50**, 1496 (1992).
G. Colò, private communications.
- [25] T. Suzuki, H. Sagawa and Nguyen Van Giai, Phys. Rev. **C57**, 139 (1998).
- [26] I. Hamamoto and H. Sagawa, Phys. Rev. **C60**, 064314 (2000).
- [27] H. de Vries, C. W. de Jager and C. de Vries. Atomic Data and Nuclear Data Tables **36**, 495(1987).
- [28] S. Drożdż, F. Osterfeld, J. Speth and J. Wambach, Phys. Lett. **B189**, 271 (1987).
- [29] H. Akimune, I. Daito, Y. Fujita, M. Fujiwara, M. N. Harakeh, J. Janecke and M. Yosoi, Phys. Rev. **C61**, 011304(R) (2000).
- [30] S. A. Long et al., Phys. Rev. **C57**, 3191(1997).